

Improving machine learning-derived photometric redshifts and physical property estimates using unlabelled observations

Humphrey, A.,^{1,2*} Cunha, P. A. C.^{1,3} Paulino-Afonso, A.,¹ Amantidis, S.,⁴ Carvajal, R.,^{5,6} Gomes, J. M.,¹ Matute, I.,^{5,6} Papaderos, P.^{5,6}

¹ *Instituto de Astrofísica e Ciências do Espaço, Universidade do Porto, CAUP, Rua das Estrelas, Porto, 4150-762, Portugal*

² *DTx – Digital Transformation CoLAB, Building 1, Azurém Campus, University of Minho, 4800-058 Guimarães, Portugal*

³ *Faculdade de Ciências da Universidade do Porto, Rua do Campo de Alegre, 4150-007 Porto, Portugal*

⁴ *Institut de Radioastronomie Millimétrique (IRAM), Avenida Divina Pastora 7, Local 20, E-18012, Granada, Spain*

⁵ *Departamento de Física, Faculdade de Ciências, Universidade de Lisboa, Edifício C8, Campo Grande, PT1749-016 Lisboa, Portugal*

⁶ *Instituto de Astrofísica e Ciências do Espaço, Faculdade de Ciências, Universidade de Lisboa, Tapada da Ajuda, PT-1349-018 Lisboa, Portugal*

Accepted 5 December 2022. Received 15 November 2022; in original form 9 June 2022

ABSTRACT

In the era of huge astronomical surveys, machine learning offers promising solutions for the efficient estimation of galaxy properties. The traditional, ‘supervised’ paradigm for the application of machine learning involves training a model on labelled data, and using this model to predict the labels of previously unlabelled data. The semi-supervised ‘pseudo-labelling’ technique offers an alternative paradigm, allowing the model training algorithm to learn from both labelled data and as-yet unlabelled data. We test the pseudo-labelling method on the problems of estimating redshift, stellar mass, and star formation rate, using COSMOS2015 broad band photometry and one of several publicly available machine learning algorithms, and we obtain significant improvements compared to purely supervised learning. We find that the gradient-boosting tree methods `CatBoost`, `XGBoost`, and `LightGBM` benefit the most, with reductions of up to $\sim 15\%$ in metrics of absolute error. We also find similar improvements in the photometric redshift catastrophic outlier fraction. We argue that the pseudo-labelling technique will be useful for the estimation of redshift and physical properties of galaxies in upcoming large imaging surveys such as *Euclid* and LSST, which will provide photometric data for billions of sources.

Key words: methods: statistical – galaxies: photometry – galaxies: fundamental parameters – galaxies: distances and redshifts

1 INTRODUCTION

The Universe and its evolution cannot be understood without first understanding galaxies, and their evolution. A key endeavour in extragalactic astrophysics is the estimation of the redshift and physical properties of galaxies (e.g., stellar mass, star-formation rate, etc.), thereby allowing galaxies to be placed in evolutionary sequences and frameworks, and facilitating the testing of galaxy evolution models (e.g., Förster Schreiber & Wuyts 2020).

Galaxy property estimation methods have traditionally used software that fits spectral templates to observed spectral energy distributions or spectra (e.g., Arnouts et al. 1999; Bolzonella, Miralles, & Pelló 2000; Cid Fernandes et al. 2005; Ilbert et al. 2006; da Cunha et al. 2008; Noll et al. 2009; Laigle et al. 2016; Gomes & Papaderos 2017; Carnall et al. 2018; Johnson et al. 2021); while generally effective and physically motivated, template fitting tends to be expensive and

often does not scale well to very large datasets (i.e., $\gg 1\text{M}$ objects), since the computation time typically scales linearly with the number of sources to be fitted.

Supervised machine learning methods represent an alternative that is increasingly applied to the problems of galaxy classification and property estimation. In this paradigm, a learning algorithm infers a function to map observations to labels, using examples of observation and label pairs. The function is subsequently used to predict the labels of new (unlabelled) examples (see, e.g., Baron 2019). A major benefit of such methods is their usually greater scalability compared to template fitting methods: Once trained, machine learning models can usually be applied to large volumes of unlabelled data at a negligible computational cost (e.g., Hemmati et al. 2019).

There are now numerous studies using supervised machine learning in the field of extragalactic astrophysics. Among its most frequent uses is in the separation of sources into different classes, for which there is now a rich body of literature. For instance, supervised learning has been successfully used

* E-mail: andrew.humphrey@astro.up.pt (AH)

by various authors to perform binary classification with the goal of selecting sources with a specific set of characteristics (e.g., [Cavuoti et al. 2014](#)), or for multi-class problems such as star/galaxy/quasar classification (e.g., [Bai et al. 2019](#); [Clarke et al. 2020](#); [Cunha & Humphrey 2022](#))

Supervised machine learning has also been extensively used to estimate galaxy redshifts from imaging or photometric data, via regression (e.g., [Collister & Lahav 2004](#); [Brescia et al. 2013](#); [Cavuoti et al. 2017](#); [Pasquet et al. 2019](#); [Razim et al. 2021](#); [Guarneri et al. 2021](#); [Carvajal et al. 2021](#); [Cunha & Humphrey 2022](#)). While reducing the required computational time is often among the main motivations for using machine learning to estimate redshift, there are now indications that these methods can significantly outperform traditional template-fitting methods, in some regions of colour-redshift space, in terms of the accuracy estimated redshifts ([Euclid Collaboration: Desprez et al. 2020](#)).

Other key uses of supervised learning in extragalactic astronomy are the estimation galaxy physical properties (e.g., [Bonjean et al. 2019](#); [Delli Veneri et al. 2019](#); [Mucesh et al. 2021](#); [Simet et al. 2021](#)), and morphological classification of galaxies from images (e.g., [Dieleman, Willett, & Dambre 2015](#); [Huertas-Company et al. 2015](#); [Domínguez Sánchez et al. 2018](#); [Tuccillo et al. 2018](#); [Nolte et al. 2019](#); [Bowles et al. 2021](#); [Brettonnière et al. 2021](#)). A few studies have also explored schemes for combining results from traditional methods with machine learning methods, resulting in improved predictions (e.g., [Cavuoti et al. 2017](#); [Fotopoulou & Paltani 2018](#)).

One weakness of the standard supervised learning paradigm is that only labelled data can be used for model training, and potentially useful information that may exist within the unlabelled data remains invisible to, and thus unused by, the training algorithm. As such, it is interesting to consider methodologies whereby models can be trained with an awareness of the content of unlabelled test data.

The ‘pseudo-labelling’ technique is a semi-supervised machine learning method that makes use of unlabelled data to refine supervised machine learning models ([Lee 2013](#); [Slijepcevic & Scaife 2021](#)). By allowing model training to make use of information about the structure and composition of the unlabelled data, the resulting model can more accurately predict labels for this data. In this paper, we demonstrate the application of pseudo-labelling to the estimation of galaxy properties using supervised machine learning and broad-band photometry.

We begin by giving a brief overview of the pseudo-labelling methodology in §2. The data and its preprocessing are described in §3. The application of pseudo-labelling to machine-learning-based estimation of photometric redshifts is presented in §5.1. Examples of its application to the estimation of stellar mass and star formation rate are presented in §5.2. Our conclusions and final remarks are given in §6.

2 THE PSEUDO-LABELLING METHODOLOGY

Pseudo-labelling is a semi-supervised technique which may be incorporated into supervised machine-learning pipelines, leveraging information contained within unlabelled data such that stronger models may be produced ([Lee 2013](#)). The main improvements from this technique arise by allowing super-

vised learning algorithms to obtain a clearer picture of the structure of the overall dataset from which the training and hold-out data are drawn. This includes allowing the learning algorithm to recognise when ‘outlier’ examples in the training set are in fact members of a significant population that is worthwhile to model rather than to ignore.

In its simplest form, the pseudo-labelling workflow is as follows. First, a supervised machine learning model is trained on a set of labelled training data. The resulting model is then used to predict the labels for the unlabelled (test) data. Subsequently, a new, larger training set is created by appending the test data to the original training data. When creating this new training set, the examples that come from the test set are labelled with their predicted labels (the ‘pseudo-labels’). The labels associated with the original training data remain unaltered, however. This yields a significantly larger training set, where the labels used for training are now a mixture of ground-truth values, and values predicted by the aforementioned model.

A new model is trained on this new training set, and is used to predict new labels for the test set examples. This process may be repeated for an arbitrary number of iterations, each time updating the pseudo-labels to their most recent predicted values, prior to training the next model. After the desired number of iterations has been completed, the resulting model is used to make the final label predictions for the test set (and other hold-out sets, if applicable). Our pseudo-labelling workflow is illustrated in [Fig. 1](#).

A real world application of this workflow might be the prediction of photometric redshifts using broad-band photometry from the *Euclid* Wide Survey ([Euclid Collaboration: Scaramella et al. 2021](#)).

In this study, we perform 50 iterations of pseudo-labelling before stopping. This was decided in order to have a reasonable balance between computation time and number of iterations. The results presented in this work required ~ 20 h of computation time on a workstation with an Intel Core i7 11700K 8-core CPU (3.6-5.0 GHz), 32 GB of RAM, and an NVIDIA RTX A6000 48GB GPU. However, the code can also be executed without a GPU, or with less powerful hardware, with some minor modifications.

We test the pseudo-labelling methodology with five open-source learning algorithms. Three of these are gradient-boosting tree (GBT) algorithms: `CatBoostRegressor`¹ ([Prokhorenkova et al. 2018](#)), `LGBMRegressor`² ([Ke et al. 2017](#)), and `XGBoost`³ ([Chen & Guestrin 2016](#)). While there are subtle differences between them, the GBT methods all have a fundamentally similar approach to model training: they combine multiple regression trees in series, with each new tree fitting the residuals from the previous trees (‘boosting’; see [Friedman 2001](#)).

From the `Python Scikit-Learn`⁴ package ([Pedregosa et al. 2011](#)) we also use the popular tree-ensemble method `RandomForestRegressor` ([Breiman 2001](#)). This learning algorithm combines multiple weak regression trees into a single, stronger regression model by averaging the predictions from

¹ <https://catboost.ai>

² <https://lightgbm.readthedocs.io>

³ <https://xgboost.readthedocs.io>

⁴ <https://scikit-learn.org>

all the individual trees. To reduce the similarity between the constituent trees, each tree is built using a subset of the features and training examples that is selected at random (with replacement).

Also from `Scikit-Learn`, we test the distance-based method `KNeighborsRegressor`. Using the k -nearest neighbours (KNN) algorithm, this is a non-parametric supervised method, which uses the similarity (typically defined by the Euclidean distance) to training examples to predict the labels for test examples. For regression problems, label predictions are usually made by averaging the k -nearest labels from the training set, where k is an integer specified by the user.

The learning algorithms were optimized to give competitive results for the prediction problems posed herein, but were not optimized exhaustively, since a test of which algorithm performs best for galaxy physical property estimation is not the goal of this study. The Python scripts used in this work are publicly available at Github⁵.

We emphasize that this methodology differs significantly from model stacking workflows (e.g., [Wolpert 1992](#); [Zitlau et al. 2016](#); [Euclid Collaboration: Humphrey et al. 2022](#); [Cunha & Humphrey 2022](#)); whereas pseudo-labelling involves appending unlabelled data (with model-predicted labels) to the training data, stacking usually only makes use of labelled data for model training.

3 DATA AND PREPROCESSING

The dataset used in this work is derived from the COSMOS2015 multiwavelength catalogue ([Laigle et al. 2016](#)). We selected a subset of 135,374 galaxies from the catalogue using the following criteria:

- (i) Galaxies not detected in X-rays (TYPE=0);
- (ii) photometric redshifts in the range $0 < z < 9.8$;
- (iii) Y , J , and $H \leq 24$ AB mag.

These criteria were designed to (i) remove active galaxies where possible, (ii) remove sources with a problematic photometric redshift, and (iii) remove faint sources with low signal to noise photometry.

To create the features for model training, we extracted the u , B , V , r , i_+ , z_+ , Y , J , H and K_s broad band magnitudes, as measured in the $3''$ aperture. In the interest of simplicity and repeatability, we have used the COSMOS2015 `MAG_APER3` measurements without applying any transformations or corrections. All unique colour combinations were then computed, resulting in 55 features (10 magnitudes and 55 colours).

Missing values represent 0.03% of these data. At the time of writing, there is no established best-practice for imputing missing photometry for use with machine learning; many of the traditional imputation methods used by machine learning practitioners (e.g., adopting the mean or median value) have the potential to result in unphysical spectral energy distributions, particularly when a photometry value is missing due to the presence of a spectral break in the spectrum of the source. We opted to impute missing photometry values with

the maximum measured magnitude of the other galaxies in the same band (e.g., [Carvajal et al. 2021](#); [Curran 2022](#)); while this does not inform the learning algorithms that the magnitude value is a special case, it does at least place sources that have missing values at approximately correct locations within the colour-magnitude hypercube (cf. [Euclid Collaboration: Humphrey et al. 2022](#), who imputed ‘magic values’ to allow learning algorithms to treat missing values differently when beneficial).

We have adopted the COSMOS2015 values of `PHOTOZ`, `MASS_BEST`, and `SFR_BEST` as the ground truth values of the redshift, $\log_{10}(M_*/M_\odot)$, and $\log_{10}(\text{SFR})$, respectively⁶. These quantities are not ‘ground-truth’ in the conventional sense, in that they were originally produced by applying the `Le Phare` template-fitting code to 30 COSMOS2015 photometry bands ([Laigle et al. 2016](#)). As such, these quantities are subject to both random and systematic errors with respect to their ‘true’ values. Figure 2 shows histograms for photometric redshift, stellar mass, and star formation rate for the selected sample.

The dataset was then randomly split into ‘train’, ‘test’, and ‘hold-out’ sets with a 12:28:10 ratio (24%, 56%, and 20%), using the `Scikit-Learn` function `train_test_split`. The train set (or training set) is used for model training, with the ground truth labels visible to the learning algorithm. Finally, all 55 features in the three data subsets (train, test, hold-out) were standardized by removing their mean and scaling to unit variance, using the mean and standard deviation calculated from the train set.

The test set simulates unlabelled data that is to be used for pseudo-labelling; our hold-out set simulated unlabelled data that is not used for pseudo-labelling, but which we use to test how well models generalise to data that was not used for training or pseudo-labelling (note that our definition of the test and hold-out sets differs slightly from some of the literature). For the test and hold-out sets, the ground truth labels are not visible to the learning algorithms, and are used only to evaluate metrics of model performance.

4 METRICS OF MODEL QUALITY

To evaluate our regression models, we use several different metrics. In the case of photometric redshift estimation, we use the normalized median absolute deviation (NMAD) as a measure of accuracy, which we calculate as

$$\text{NMAD} = 1.48 \text{ median} \left(\frac{|z_{\text{phot}} - z_{\text{ref}}|}{1 + z_{\text{ref}}} \right), \quad (1)$$

where z_{phot} is the redshift predicted by the model, and z_{ref} is the reference photometric redshift used as the ‘ground truth’. The NMAD is roughly analogous to the standard deviation: $\sigma \approx \kappa \text{MAD}$, where MAD is the median absolute deviation, and κ is a constant scale factor; $\kappa \approx 1.48$ for normally distributed data. An advantage of the NMAD metric is that it is less affected by outliers than is the classical standard deviation.

It is also of interest to use a metric that quantifies the

⁵ <https://github.com/humphrey-and-the-machine/pseudo-labelling>. The readme file for this repository gives instructions for how to modify the code for use without a GPU, and/or with less powerful computing hardware.

⁶ In the interest of brevity, we hereinafter use M_* and SFR to mean the log of the quantities.

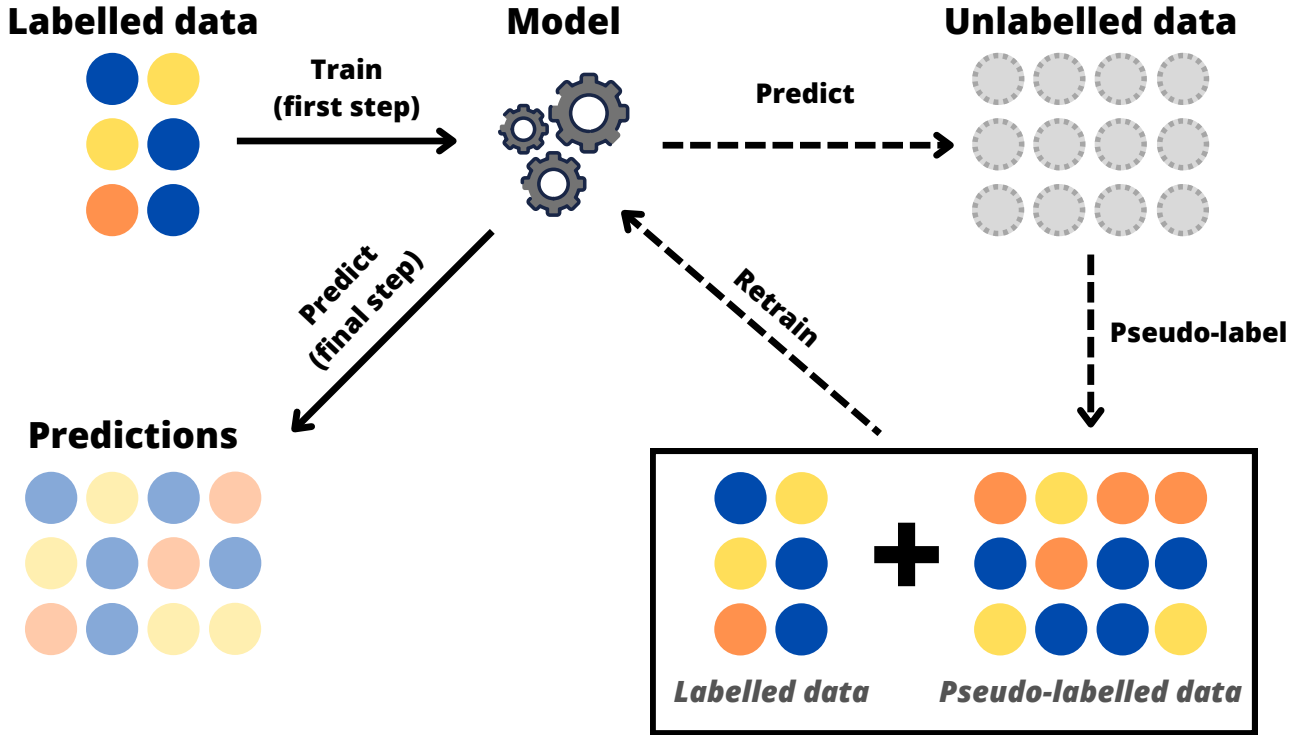


Figure 1. Flow diagram illustrating the pseudo-labelling procedure that we have used. Labelled data is used to train an initial model; the model predicts (pseudo) labels for unlabelled data; this pseudo-labelled data is appended to the training data; the resulting dataset used to train a new model, predict new labels, update the pseudo-labels, and so on, until stopping criteria are reached (50 iterations in our case).

number of outliers among the redshift predictions. Thus, we adopt the following criterion to classify redshift estimates as catastrophic outliers:

$$\frac{|z_{\text{phot}} - z_{\text{ref}}|}{1 + z_{\text{ref}}} > 0.15. \quad (2)$$

In addition, we define the bias of the photometric redshift estimates as

$$\text{bias} = \text{median} \left(\frac{z_{\text{phot}} - z_{\text{ref}}}{1 + z_{\text{ref}}} \right). \quad (3)$$

To quantify the errors in predicting M_* and SFR, we use the mean absolute error, the median absolute error, and the coefficient of determination R^2 . The mean absolute error is calculated as

$$\text{mean absolute error} = \frac{\sum_{i=1}^n (\hat{y}_i - y_i)}{n} \quad (4)$$

where y_i is the true value of the label of the i -th sample, \hat{y}_i is the predicted value, and n is the total number of samples. Similarly, the median absolute error is calculated as

$$\text{median absolute error} = \text{median} (\hat{y}_i - y_i). \quad (5)$$

The R^2 score is calculated as

$$R^2 = \frac{\sum_{i=1}^n (\hat{y}_i - y_i)^2}{\sum_{i=1}^n (y_i - \bar{y})^2} \quad (6)$$

where \bar{y} is y_i averaged over n samples. Unlike the previous metrics, higher values of R^2 indicate a better model, up to a maximum value of 1, with no minimum value.

5 RESULTS AND DISCUSSION

In Figs. 3-5, we show the evolution of selected metrics of model quality versus iteration number, when applying pseudo-labelling to the estimation of photometric redshift (Fig. 3), stellar mass (Fig. 4), and SFR (Fig. 5). Each quantity was predicted separately, using a dedicated single-output model.

The curves correspond to the metrics of model quality, averaged over 10 runs, using different random seeds. The zeroth iteration corresponds to the initial model trained using only the train set; subsequent iterations pertain to models training using pseudo-labelling. In Fig. 6, we also show the maximum improvement obtained during the 50 iterations of pseudo-labelling.

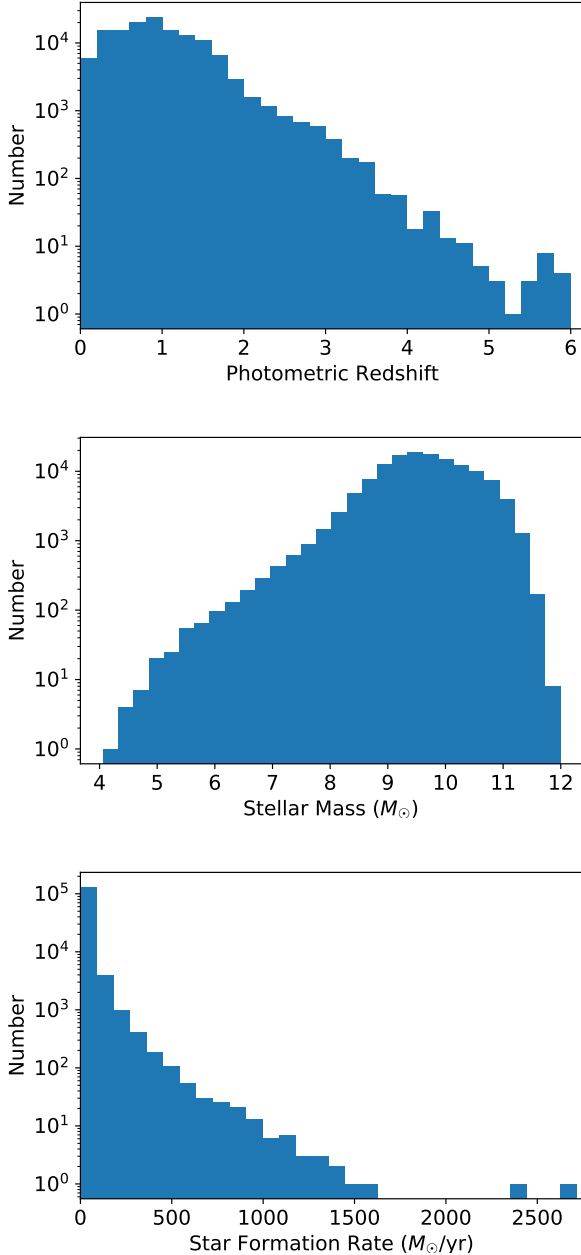


Figure 2. Histograms for photometric redshift, stellar mass, and star formation rate for the selected sample.

The behaviour of the different learning algorithms varies substantially when applying pseudo-labelling. `CatBoostRegressor`, `LightGBMRegressor`, and `XGBoostRegressor` all experienced significant improvements in model quality. Conversely, pseudo-labelling only offered a marginal improvement to the `KNeighborsRegressor` models, and appears to be significantly detrimental to the `RandomForestRegressor` models.

The reasons why the different learning algorithms respond differently to pseudo-labelling are complex, but can be thought of as to a trade-off between the enlargement of the training sample, which usually improves model quality,

and the inclusion of some incorrect (pseudo) labels, which can degrade model quality (e.g., [Euclid Collaboration: Humphrey et al. 2022](#)). A more detailed description of the results is given in the following subsections.

5.1 Photometric redshift

5.1.1 Gradient boosted tree models

It is clear from Fig. 3 that pseudo-labelling can significantly improve the NMAD and outlier fraction metrics for photometric redshift estimates, but this depends on the learning algorithm used, and on the number of iterations of pseudo-labelling that are performed.

The greatest improvements ($\gtrsim 5\%$) are obtained when using a gradient boosted tree method (GBT; `CatBoost`, `LightGBM`, or `XGBoost`; see the first 3 rows of Figs. 3-5). In these cases, the NMAD decreases rapidly in the first ~ 3 iterations of pseudo-labelling, after which the NMAD curve either flattens-off (`CatBoost`), experiences an up-turn (`LightGBM`), or continues in a gradual decline (`XGBoost`). All three GBT algorithms show a broadly similar evolution in the catastrophic outlier fraction, with an initially steep decline that becomes shallower as the pseudo-labelling iterations proceed.

A noteworthy result is that the improvements in the NMAD and outlier fraction of the test set predictions are accompanied by improvements in the hold-out set predictions (see, e.g., Fig. 3 panels a,b), indicating that improved generalisation was achieved not only for the test set (used for the pseudo-labelling), but also to the hold-out set (not involved in model training). However, the improvements in NMAD and outlier fraction are smaller for the hold-out set than for the test set.

The initial models (zeroth iteration) result in predictions with a generally low redshift bias, which the pseudo-labelling process further improves in the cases of `CatBoost` and `XGBoost`.

5.1.2 Other models

The results from using pseudo-labelling with the other learning algorithms (`KNeighborsRegressor` or `RandomForestRegressor`) are less clear-cut. In the case of `KNeighborsRegressor` (Fig. 3 panels d,j,p), the first ~ 2 iterations provide only a marginal improvement in NMAD, while the outlier fraction shows a sharp initial decrease followed by a reversal back up towards, but not reaching, the starting value. A marginal improvement is also present in the bias.

The `RandomForestRegressor` (Fig. 3 panels f,l,r) stands out as the learning algorithm that did not receive any benefit from pseudo-labelling. Even from the first iteration of pseudo-labelling, the values of the NMAD, outlier fraction, and bias are always significantly higher than when pseudo-labelling is not used (the zeroth iteration). In effect, we see a gradual accumulation of errors due to the introduction of label noise.

5.2 Stellar mass and SFR

The results from applying pseudo-labelling to the estimation of M_* (Fig. 4) and SFR (Fig. 5) are broadly analogous to

Photometric Redshift

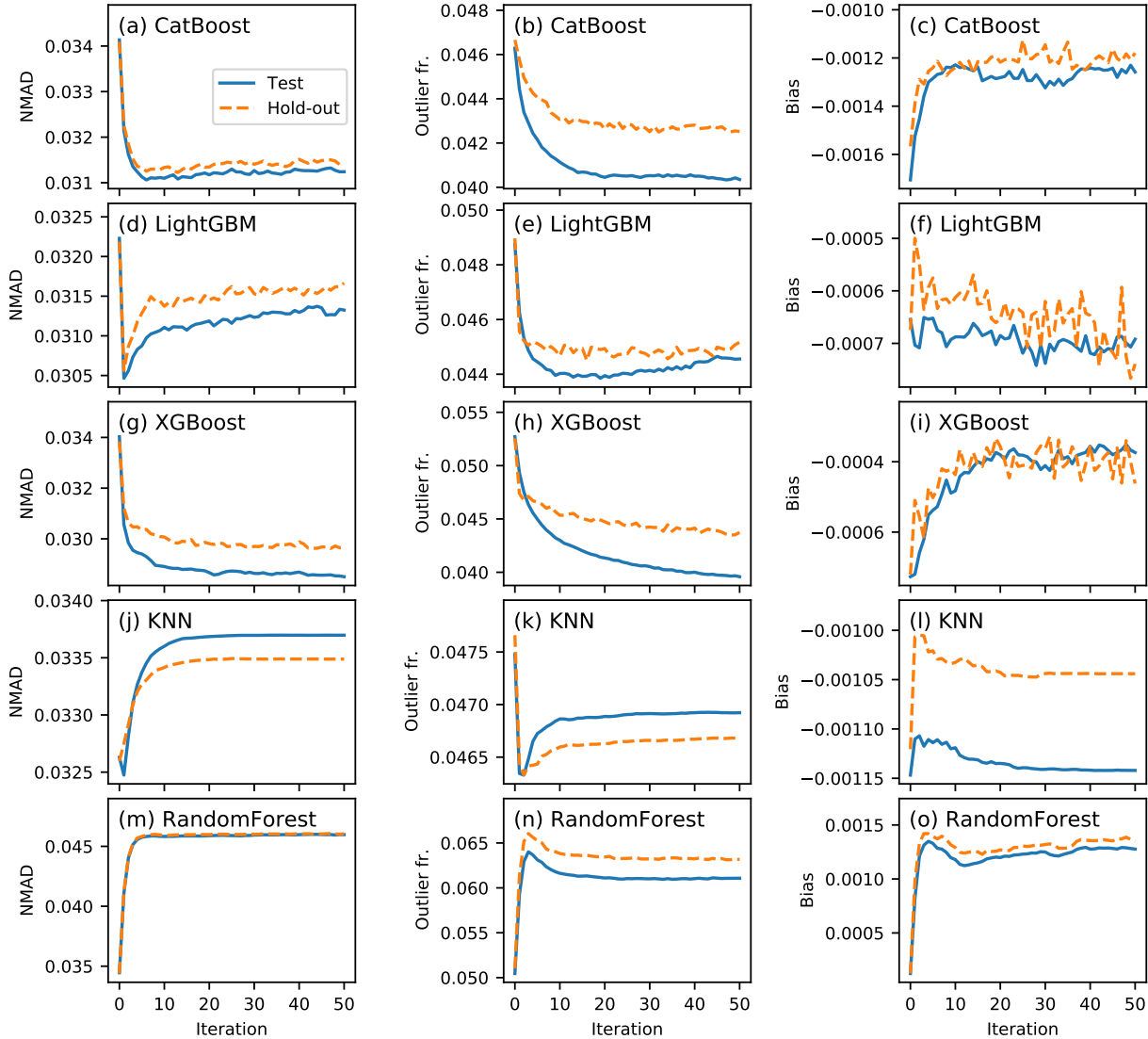


Figure 3. Estimating photometric redshifts using pseudo labelling with `CatBoost`, `LightGBM`, `XGBoost`, `KNeighborsRegressor` or `RandomForestRegressor`. The zeroth iteration corresponds to the initial model trained only on the training set; the subsequent 50 iterations correspond to the pseudo-labelling process. The solid blue line shows the evolution of the photometric redshift metrics as a function of the pseudo labelling iteration, for the test set used for pseudo-labelling. The dashed orange shows the evolution of the metrics for the hold-out set, which was not used for model training or pseudo labelling. The results shown in this figure correspond to the averaged metrics from 10 runs with different random seeds for the random train / test / hold-out split, and where applicable, for the learning algorithms also. Left column: Normalised median absolute deviation. Middle column: Catastrophic outlier fraction. Right column: The overall bias of the prediction errors.

those described in §5.1. For the GBT methods, there is a rapid decrease in mean absolute error and median absolute error values during the initial ~ 5 iterations of pseudo-labelling. The subsequent evolution in these two metrics differs between the three GBT methods. In the case of `CatBoost`, a constant value is quickly reached. For (`LightGBM`), there is a reversal and increase in the metric values. In the case of `XGBoost`, the

metric values continue their gradual decrease, albeit with a shallower gradient. Likewise, the R^2 scores when using the GBT methods show an initially significant increase in model quality (higher values), followed by an evolution that depends on which learning algorithm was used.

For `KNeighborsRegressor` the test set predictions improve marginally after a single iteration of the pseudo-labelling pro-

Log Stellar Mass

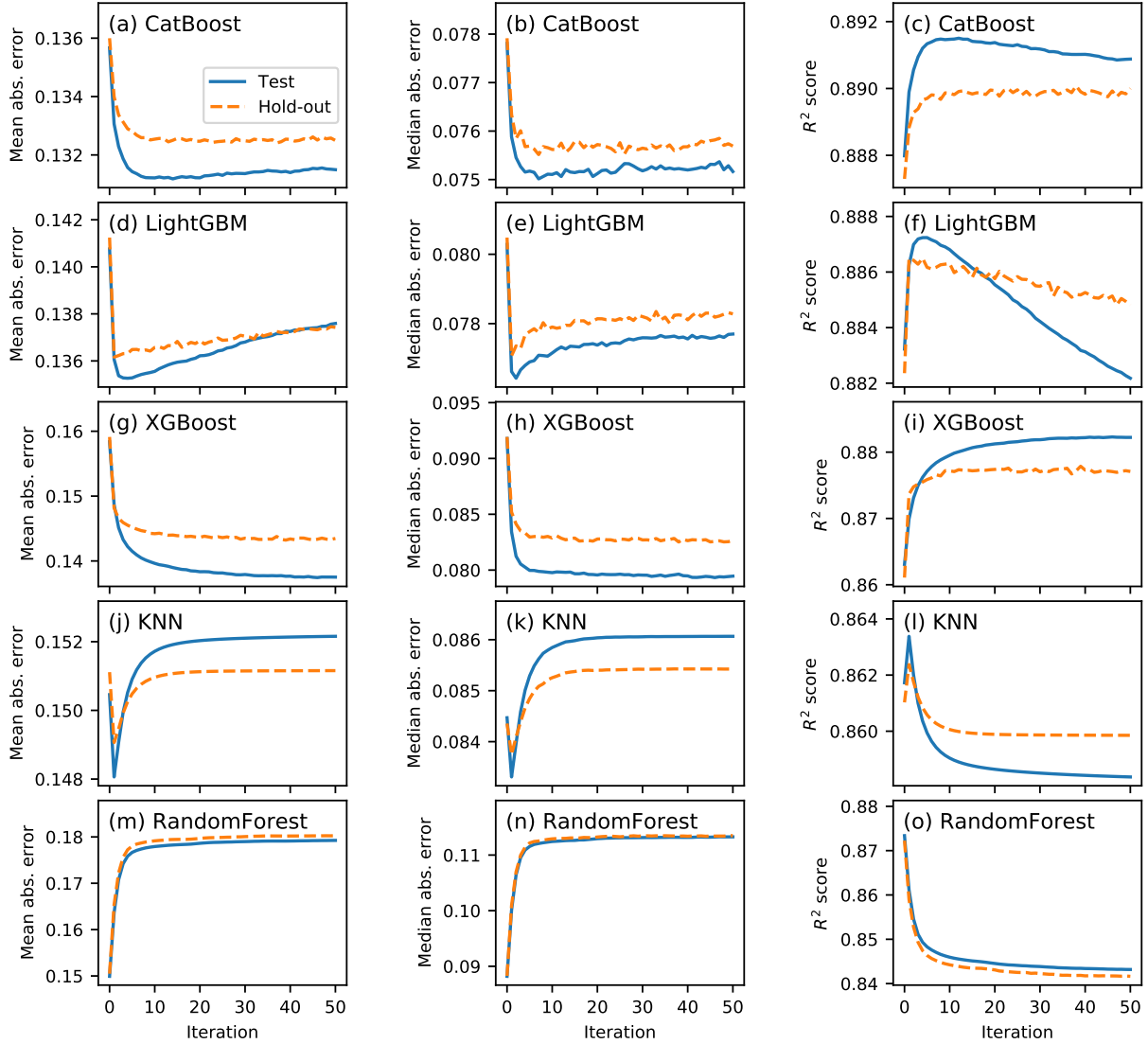


Figure 4. Similar to Fig. 3, but for the estimation of $\text{Log}_{10}M_*$. Left column: Mean absolute error. Middle column: Median absolute error. Right column: R^2 score.

cedure, as shown by the decrease in the mean absolute error, median absolute error, and R^2 score. However, from the second iteration onward model quality diminishes, such that by the tenth iteration the aforementioned metrics have values that are significantly worse than the initial (zeroth iteration) model. For the hold-out set, we find little, if any, improvement in model quality with the application of pseudo-labelling.

Similar to the results for photometric redshift estimation, in the case of **RandomForest** the mean absolute error, median absolute error, and R^2 score show a substantial reduction in model quality as the result of application of pseudo-labelling.

6 CONCLUDING REMARKS

We have explored the application of the semi-supervised pseudo-labelling methodology to the problem of estimating galaxy redshift, stellar mass, and star-formation rate from broad band photometry and colours. The dataset used is derived from the COSMOS2015 multiwavelength catalogue of [Laigle et al. \(2016\)](#). Our tests simulate the case of a photometric dataset produced by a large-scale imaging survey, for which labels are available only for a small subset of the sources; the objective is to examine whether pseudo-labelling can be used to improve machine learning models for the pre-

Log Star Formation Rate

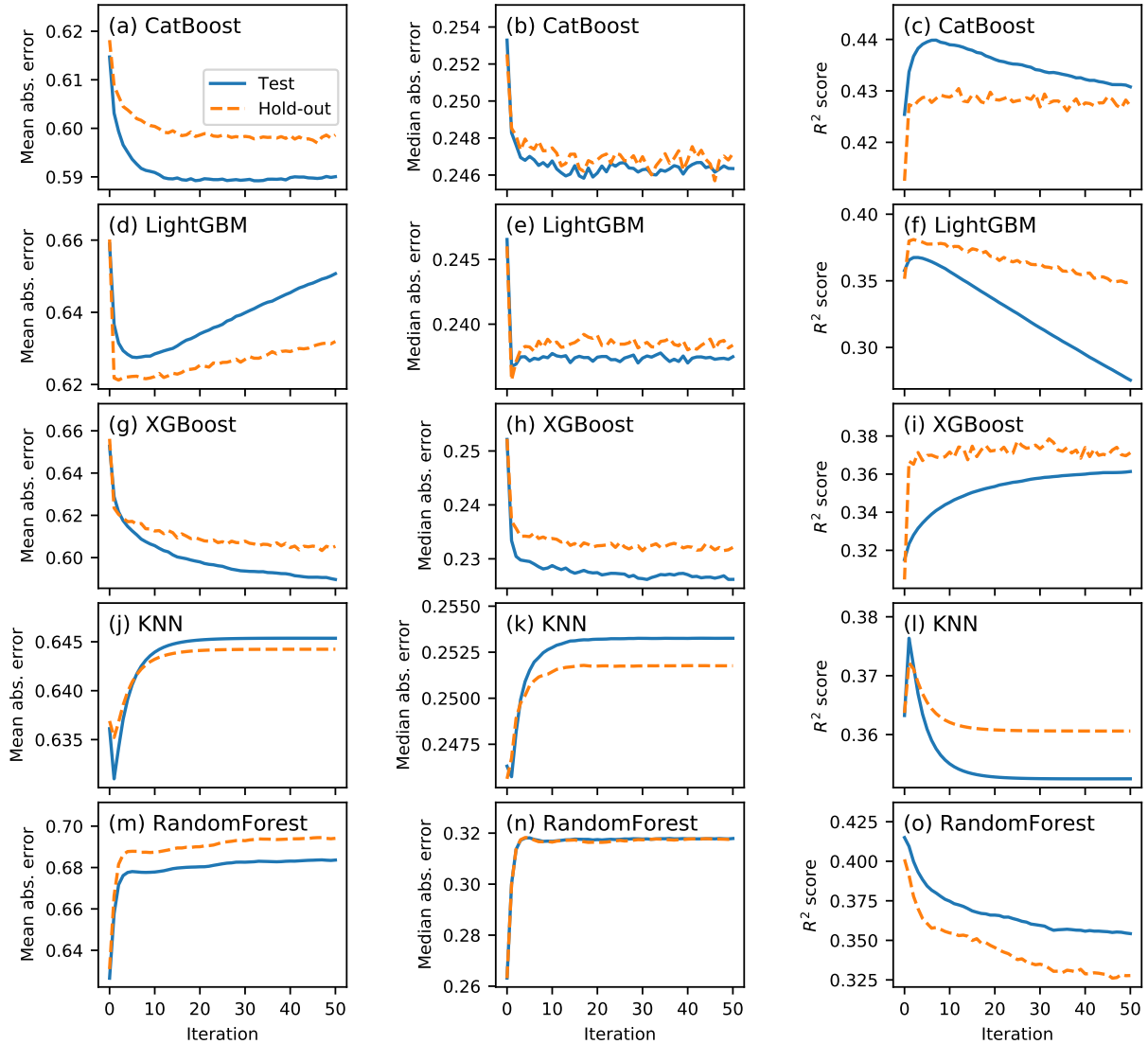


Figure 5. Similar to Figs. 3 and 4, but for the estimation of $\text{Log}_{10}\text{SFR}$.

diction of the missing labels, compared to the simple case where only the labelled data is used for model training.

We have demonstrated that our methodology can result in regression models that are able to predict redshift, stellar mass, and star-formation rate significantly more accurately, with typical improvements in metrics of absolute error of $\sim 5\text{--}15\%$, by making use of information present in unlabelled data.

In cases where improved predictions are obtained for the test data used for the pseudo-labelling, the predictions for hold-out data (not used for pseudo-labelling) also show significant, but typically smaller, improvement. In other words, pseudo-labelling also results in improved generalisation to previously unseen hold-out data.

An important caveat that must be stated is that the per-

formance of our implementation of pseudo-labelling, in terms of how well it improves supervised machine learning models for galaxy properties, depends on the learning algorithm with which it is used. For instance, we find that models produced with the gradient boosting tree methods `CatBoostRegressor`, `LightGBMRegressor`, and `XGBoostRegressor` experience the greatest improvements from the use of pseudo-labelling. Conversely, models trained with the popular tree-ensemble method `RandomForestRegressor` were negatively affected by the application pseudo-labelling.

This study is intended to be a proof-of-concept for the use of pseudo-labelling for the estimation of the properties of astronomical sources. As such, we have not exhaustively tested all available learning algorithms, nor have we exhaustively

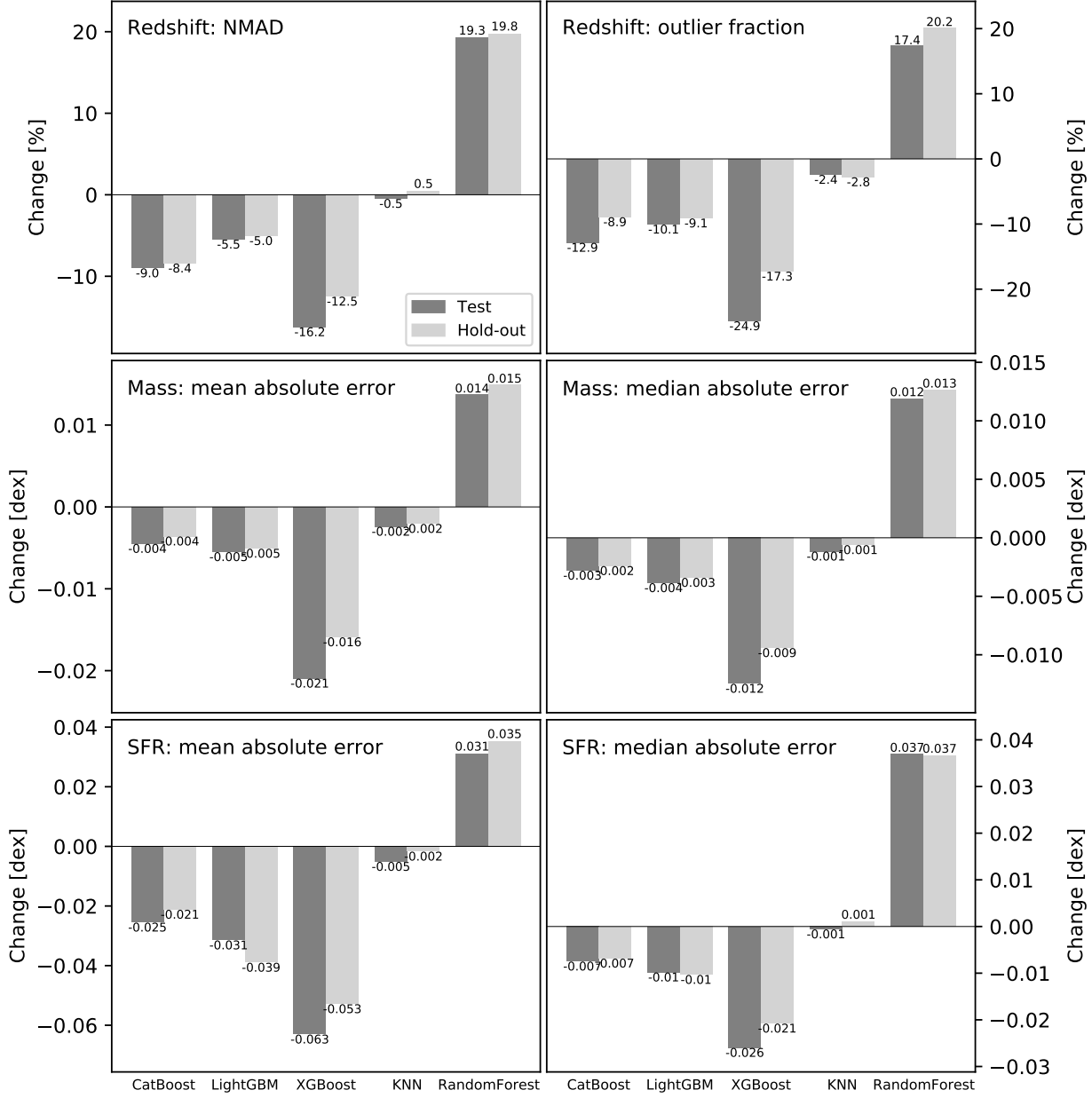


Figure 6. Quantifying the improvement, if any, obtained by applying pseudo-labelling. Each panel shows the maximum improvement obtained, relative to the zeroth iteration, for each learning algorithm, during the 50 iterations of pseudo-labelling. Negative values (i.e., reduced errors) indicate an improvement, and positive values indicate that model quality worsened.

optimised the hyperparameters of the learning algorithms we use herein. In a future study, we will explore in greater detail the application of pseudo-labelling (and other variants thereof) to the classification and property estimation of astronomical sources.

Finally, we emphasize that the pseudo labelling technique is likely to be useful for enhancing the quality of estimates of galaxy redshift and physical properties in large upcoming (and ongoing) imaging surveys such as UNIONS (Chambers et al. 2020), LSST (Ivezić et al. 2019) and *Euclid* (Laureijs et al. 2011), which will produce rich, but challengingly vast datasets in need of computationally efficient labelling.

ACKNOWLEDGEMENTS

We thank the referee for their careful reviews and useful comments. This work was supported by Fundação para a Ciência e a Tecnologia (FCT) through grants UID/FIS/04434/2019, UIDB/04434/2020, UIDP/04434/2020 and PTDC/FIS-AST/29245/2017, EXPL/FIS-AST/1085/2021, and an FCT-CAPES Transnational Cooperation Project. R.C. acknowledges support from the FCT through the Fellowship PD/BD/150455/2019 (PhD:SPACE Doctoral Network PD/00040/2012). We also acknowledge support from NVIDIA in the form of a GPU under the NVIDIA Academic

Hardware Grant Program. In the development of this work, we have made use of the `Pandas` (McKinney 2010), `Numpy` (Harris et al. 2020), and `Dask` (Rocklin 2015) packages for Python.

DATA AVAILABILITY

All data and methods used in this study are publicly available at <https://github.com/humphrey-and-the-machine>.

REFERENCES

- Arnouts, S., Cristiani, S., Moscardini, L., et al. 1999, *MNRAS*, 310, 540
- Bai, Y., Liu, J., Wang, S., et al. 2019, *AJ*, 157, 9
- Baron, D. 2019, arXiv:1904.07248
- Bolzonella, M., Miralles, J.-M., & Pelló, R. 2000, *A&A*, 363, 476
- Bonjean, V., Aghanim, N., Salomé, P., et al. 2019, *A&A*, 622, A137
- Bowles, M., Scaife, A. M. M., Porter, F., Tang, H., & Bastien, D. J. 2021, *MNRAS*, 501, 4579
- Breiman, L. 2001, *Mach. Learn.*, 45, 1
- Brescia, M., Cavuoti, S., D’Abrusco, R., Longo, G., & Mercurio, A. 2013, *ApJ*, 772, 140
- Bretonnière, H., Boucaud, A., & Huertas-Company, M. 2021, arXiv:2111.15455
- Carnall, A. C., McLure, R. J., Dunlop, J. S., et al. 2018, *MNRAS*, 480, 4379
- Carvajal, R., Matute, I., Afonso, J., et al. 2021, *Galaxies*, 9, 86
- Cavuoti, S., Tortora, C., Brescia, M., et al. 2017, *MNRAS*, 466, 2039
- Cavuoti, S., Brescia, M., D’Abrusco, R., Longo, G., & Paolillo, M. 2014, *MNRAS*, 437, 968
- Chambers, K., Unions Team including Pan-Starrs Team, & CFIS Team 2020, American Astronomical Society meeting 235, id. 154.04. *Bulletin of the American Astronomical Society*, Vol. 52, No. 1
- Chen, T., Guestrin, C., 2016 arXiv:1603.02754v3
- Cid Fernandes, R., Mateus, A., Sodré, L., et al. 2005, *MNRAS*, 358, 363
- Clarke, A. O., Scaife, A. M. M., Greenhalgh, R., & Griguta, V. 2020, *A&A*, 639, A84
- Collister, A. A., & Lahav, O. 2004, *PASP*, 116, 345
- Cunha, P. A. C. & Humphrey, A. 2022,
- da Cunha, E., Charlot, S., & Elbaz, D. 2008, *MNRAS*, 388, 1595
- Curran, S. J. 2022, *MNRAS*, 512, 2099
- Delli Veneri, M., Cavuoti, S., Brescia, M., Longo, G., & Riccio, G. 2019, *MNRAS*, 486, 1377
- Dieleman, S., Willett, K. W., & Dambre, J. 2015, *MNRAS*, 450, 1441
- Domínguez Sánchez, H., Huertas-Company, M., Bernardi, M., et al. 2018, *MNRAS*, 476, 3661
- Euclid Collaboration: Desprez, G., Paltani, S., et al. 2020, *A&A*, 644, A31
- Euclid Collaboration: Humphrey A., Bisigello L., Cunha P. A. C., Bolzonella M., Fotopoulou S., Caputi K., Tortora C., et al., 2022, *A&A*, accepted. arXiv:2209.13074
- Euclid Collaboration, Scaramella, R., Amiaux, J., et al. 2022, *A&A*, 662, A112
- Friedman J., 2001, *The Annals of Statistics*, Vol. 29, No. 5
- Förster Schreiber, N. M. & Wuyts, S. 2020, *ARA&A*, 58, 661
- Fotopoulou, S., & Paltani, S. 2018, *A&A*, 619, A14
- Gomes, J. M., & Papaderos, P. 2017, *A&A*, 603, A63
- Guarneri, F., Calderone, G., Cristiani, S., et al. 2021, *MNRAS*, 506, 2471
- Harris, C. R., Millman, K. J., van der Walt, S. J., et al. 2020, *Nature*, 585, 357
- Hemmati, S., Capak, P., Pourrahmani, M., et al. 2019, *ApJ*, 881, L14
- Huertas-Company, M., Gravet, R., Cabrera-Vives, G., et al. 2015, *ApJS*, 221, 8
- Ilbert, O., Arnouts, S., McCracken, H. J., et al. 2006, *A&A*, 457, 841
- Ivezić, Ž., Kahn, S. M., Tyson, J. A., et al. 2019, *ApJ*, 873, 111
- Johnson, B. D., Leja, J., Conroy, C., et al. 2021, *ApJS*, 254, 22
- Ke, G., Meng, Q., Finley, T., Wang, T., Chen, W., Ma, W., Ye, Q., and Liu, T.-Y., 2017, *LightGBM: A Highly Efficient Gradient Boosting Decision Tree*, in *Advances in Neural Information Processing Systems*, vol. 30, 3146
- Laigle, C., McCracken, H. J., Ilbert, O., et al. 2016, *ApJS*, 224, 24
- Laureijs, R., Amiaux, J., Arduini, S., et al. 2011, [arXiv:1110.3193]
- Lee, D., “Pseudo-Label: The Simple and Efficient Semi-Supervised Learning Method for Deep Neural Networks.” *ICML 2013 Workshop: Challenges in Representation Learning (WREPL)*, Atlanta, Georgia, USA, 2013 [eprint]
- McKinney, w., 2010, *Data Structures for Statistical Computing in Python*, in *Proceedings of the 9th Python in Science Conference*, pp 51
- Mucesh, S., Hartley, W. G., Palmese, A., et al. 2021, *MNRAS*, 502, 2770
- Noll, S., Burgarella, D., Giovannoli, E., et al. 2009, *A&A*, 507, 1793
- Nolte, A., Wang, L., Bilicki, M., Holwerda, B., & Biehl, M. 2019, arXiv e-prints, arXiv:1903.07749
- Pasquet, J., Bertin, E., Treyer, M., et al. 2019, *A&A*, 621, A26
- Pedregosa, F., et al., 2011, *Journal of Machine Learning Research*, 12, 2825
- Prokhorenkova, L., Gusev, G., Vorobev, A., Dorogush, A.V., Gulin, A., 2018, *Advances in Neural Information Processing Systems*, 31, 6638
- Razim, O., Cavuoti, S., Brescia, M., Riccio, G., Salvato, M., Longo, G., 2021, *MNRAS*, 507, 5034
- Rocklin, M., 2015, *Dask: Parallel Computation with Blocked Algorithms and Task Scheduling*, in *Proceedings of the 14th Python in Science Conference*, pp 130
- Simet, M., Chartab, N., Lu, Y., & Mobasher, B. 2021, *ApJ*, 908, 47
- Slijepcevic, I. V. & Scaife, A. M. M. 2021, arXiv:2111.04357
- Tuccillo, D., Huertas-Company, M., Decencièrre, E., et al. 2018, *MNRAS*, 475, 894
- Zitlau, R., Hoyle, B., Paech, K., et al. 2016, *MNRAS*, 460, 3152
- Wolpert, D.H. 1992, *Neural Networks*, 5(2), 241-259

This paper has been typeset from a $\text{\TeX}/\text{\LaTeX}$ file prepared by the author.